Available online at www.sciencedirect.com
SCIENCE DIRECT
Journal of Power Sources 150 (2005) 261–271
JOURNAL OF POWER SOURCES
www.elsevier.com/locate/jpowsour

The electrochemical properties of Fe_2O_3-loaded carbon electrodes for iron–air battery anodes

Bui Thi Hang [a,*], Tomonori Watanabe [a], Minato Eashira [b,1], Shigeto Okada [b], Jun-ichi Yamaki [b], Satoshi Hata [c], Seong-Ho Yoon [b], Isao Mochida [b]

[a] *Interdisciplinary Graduate School of Engineering Sciences, Kyushu University, 6-1 Kasuga-koen, Fukuoka 816-8580, Japan*
[b] *Institute for Materials Chemistry and Engineering, Kyushu University, 6-1 Kasuga-koen, Fukuoka 816-8580, Japan*
[c] *Department of Engineering Science for Electronics and Materials, Kyushu University, 6-1 Kasuga-koen, Fukuoka 816-8580, Japan*

Received 14 January 2005; received in revised form 21 February 2005; accepted 28 February 2005
Available online 5 April 2005

Abstract

The redox efficiency of iron has been improved by increasing the distribution of iron on the carbon surface with Fe_2O_3-loaded carbon materials. The Fe_2O_3-loaded carbon material was prepared by loading Fe_2O_3 on carbon by a chemical method. $Fe(NO_3)_3$ was impregnated on carbon with different weight ratios of iron-to-carbon in an aqueous solution, and the mixture was dried and then calcined for 1 h at 400 °C in flowing Ar. The effect of various carbons on the physical and electrochemical properties of Fe_2O_3-loaded carbon electrodes was investigated with the use of X-ray diffraction (XRD), transmission electron microscopy (TEM), scanning electron microscopy (SEM) along with X-ray energy-dispersive spectroscopy (EDS), cyclic voltammetry (CV) and galvanostatic cycling performance. Transmission electron microscopy coupled with X-ray diffraction measurements revealed that small Fe_2O_3 particles were distributed on the carbon surface. Natural graphite and several nano-carbon materials such as acetylene black and tubular carbon nanofibers (tubular CNF) exhibited improved characteristics, such as enhanced capacity and higher redox currents for the Fe_2O_3-loaded carbon electrode. SEM and EDS results suggest that Fe_2O_3-loaded nano-carbon electrodes, due to the large surface area of the nano-carbon, have more Fe_2O_3 dispersed than on Fe_2O_3-coated graphite electrodes.

Keywords: Nano-carbon; Fe_2O_3-loaded carbon materials; Iron–air battery anode

1. Introduction

High energy density for metal/air batteries has been the focus of attention [1–3] in recent years for applications involving electric vehicles, among others. The anode in an air battery plays a key role in deciding the performance, especially the specific capacity and cycle life. Three kinds of air batteries are interesting, viz., Fe/air, Zn/air and Al/air. However, all of these air batteries have some disadvantages due to the anode. For example, a zinc anode can experience an inhomogeneous distribution of deposition during charging, resulting in a "shape change" phenomenon, leading to loss of cycle life. An aluminum anode is only mechanically rechargeable. On the other hand, the iron anode forms a passive layer during the discharge process. Much research has been involved with improving these anodes. In recent years, iron electrodes have received considerable attention [4–22], in view of their high theoretical capacity (0.96 Ah g^{-1}), long cycle life and low cost, in addition to having good resistance towards mechanical shock, vibrations, over-charge and deep discharge [18]. However, in practice, the porous iron electrode presents low charge efficiency, since the hydrogen evolution reaction competes with the discharge reaction [18]. In order to improve

* Corresponding author. Tel.: +81 92 583 7841; fax: +81 92 583 7790.
E-mail address: hang@cm.kyushu-u.ac.jp (B.T. Hang).
[1] Present address: Faculty of Engineering, Yamaguchi University 2-16-1, Tokiwadai, Ube, Yamaguchi 755-8611, Japan.

0378-7753/$ – see front matter © 2005 Elsevier B.V. All rights reserved.
doi:10.1016/j.jpowsour.2005.02.028

Table 1
Main characteristics of the carbon materials

	Grain size (nm)	BET surface area ($m^2\,g^{-1}$)	True density ($g\,cm^{-3}$)
VGCF	100–300	13	2.21
AB	40–100	68	2.0
Natural graphite	18000	8	2.24
Tubular CNF	20–100	92	2.09
Platelet CNF	40–200	91	2.10

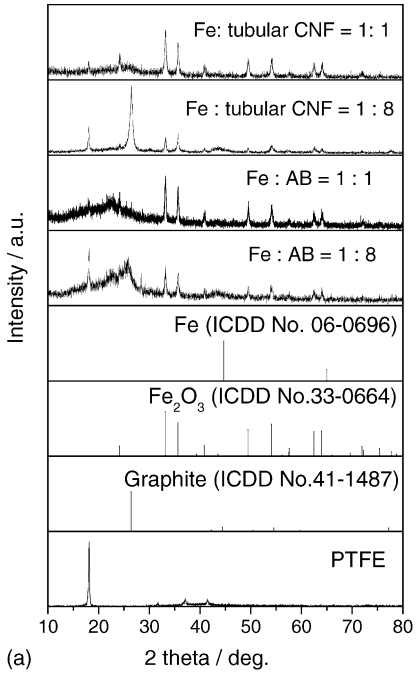

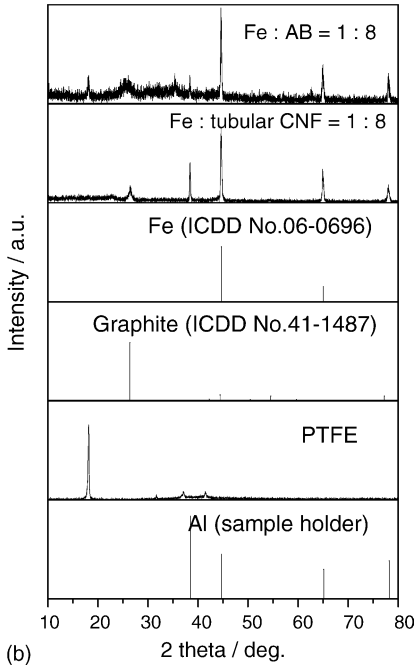

Fig. 1. X-ray pattern of Fe_2O_3-loaded AB and Fe_2O_3-loaded tubular CNF before (a) and after (b) cycling for different weight ratios of iron-to-carbon.

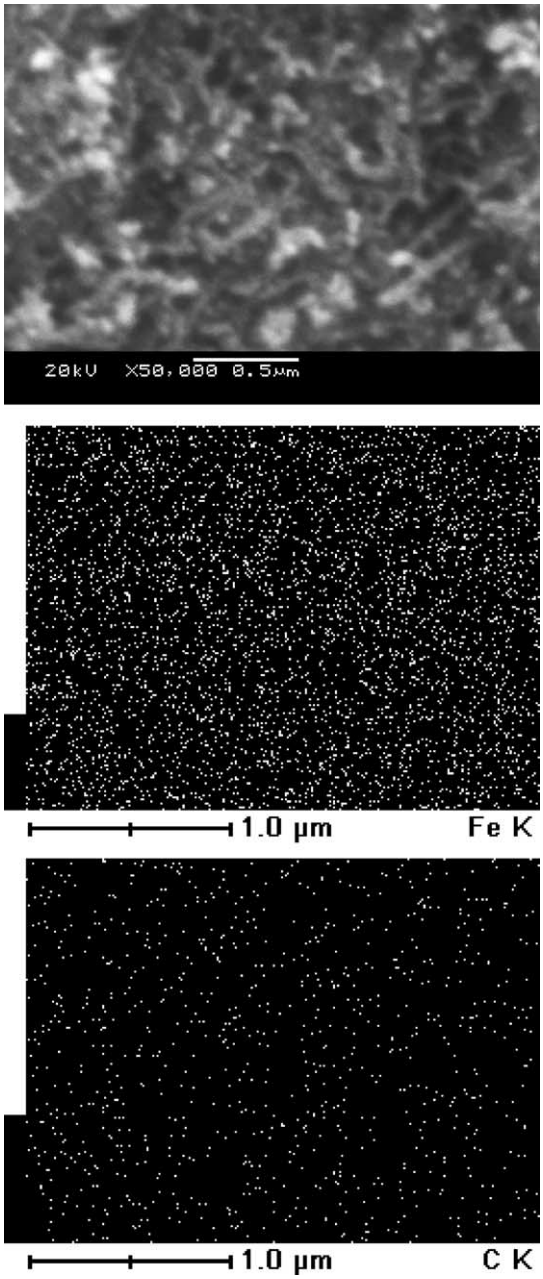

Fig. 2. SEM images and distribution of Fe_2O_3 and carbon of Fe_2O_3-loaded tubular CNF material.

the passivation of the iron electrode during the galvanostatic cycling, various kinds of carbons were used for preparing Fe/C electrodes for use as anodes in Fe/air batteries [23]. Recently, the authors reported that the Fe/nano-carbon-mixed composite electrode showed improved charge–discharge performance [23]. However, in preparing such composite materials, it is preferable that the contact between iron and carbon be maximized. In order to increase the active material surface area, in the present study, we present the preparation of a novel Fe_2O_3-loaded carbon composite electrode, using various carbon materials, for use as an anode in Fe/air batteries.

2. Experimental

Vapor-grown carbon fibers (VGCF; Showa Denko Co.), acetylene black (AB; Denki Kagaku Co.) and natural graphite (Chuetsu Graphite Co.), with average diameters of ca. 200, 100 nm and 18 μm, respectively, were used in the present work. In addition, two kinds of carbon nanofibers (CNFs), of the nanotube type, having an average diameter of ca. 50 nm, and a platelet type, having an average diameter of ca. 150 nm, were also investigated. For tubular CNF, hexagonal planes compose hollow tubes, while in platelet CNF, a smaller hexagonal plane is stacked perpendicular to the fiber axis. The main characteristics of the carbon materials employed are listed in Table 1; their morphology has been described in our previous work [23]. Iron nitrate (Wako Pure Chemical Co.) was used as the iron source.

The Fe_2O_3-loaded carbon material was prepared by loading Fe_2O_3 on carbon, as described below. $Fe(NO_3)_3$ was impregnated on carbon with various weight ratios of

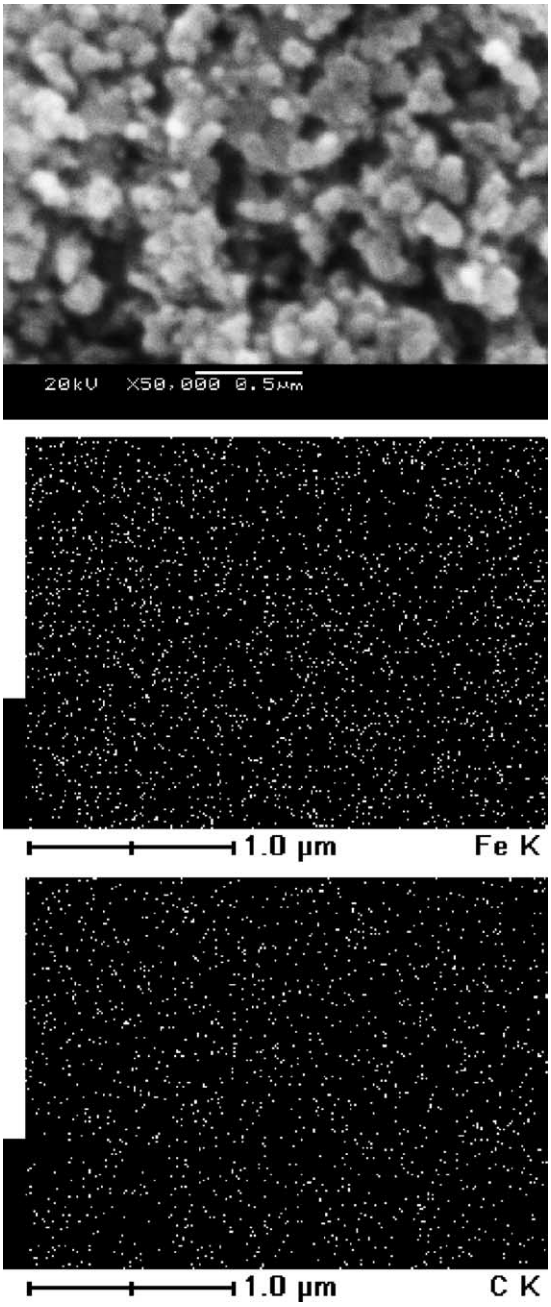

Fig. 3. SEM images and distribution of Fe_2O_3 and carbon of Fe_2O_3-loaded AB material.

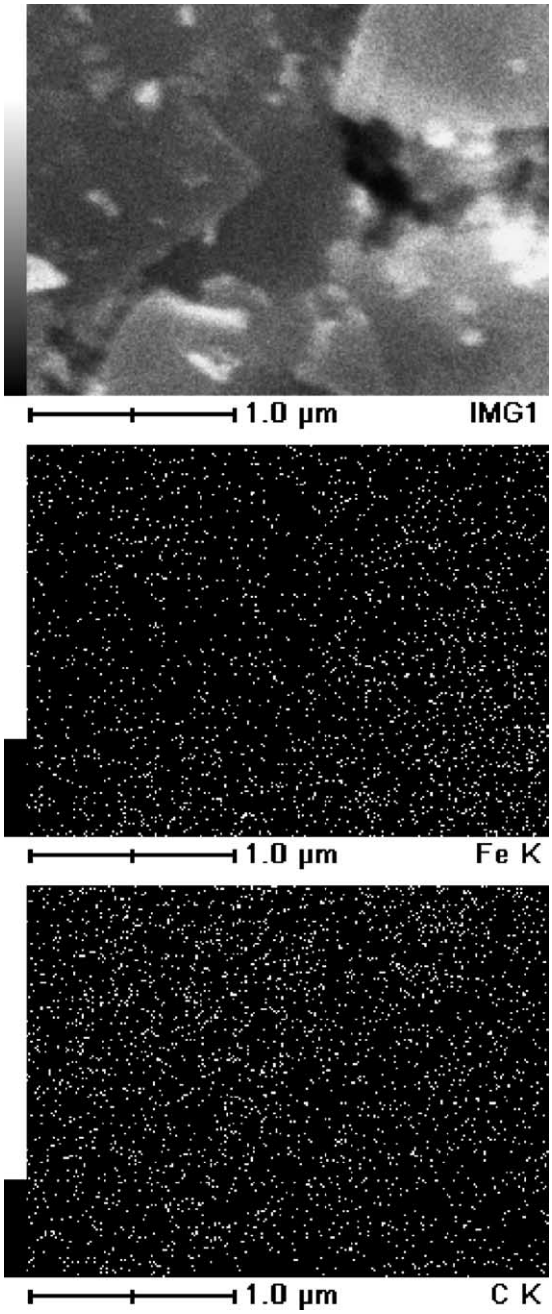

Fig. 4. SEM images and distribution of Fe_2O_3 and carbon of Fe_2O_3-loaded natural graphite material.

iron-to-carbon (1:1, 1:2, 1:4 and 1:8) in an aqueous solution, and the mixture was dried at 70 °C, followed by calcination for 1 h at 400 °C in flowing Ar. The Fe compound obtained on the carbons was identified to be Fe_2O_3 by X-ray diffraction (XRD). The morphology of the as-prepared Fe_2O_3-loaded carbon materials was observed by transmission electron microscopy (TEM), and scanning electron microscopy (SEM) together with X-ray energy-dispersive spectroscopy (EDS). X-ray measurements were also carried out on these materials.

In order to obtain the electrochemical behavior of each Fe_2O_3-loaded carbon material, an electrode sheet was prepared by mixing 90 wt.% of the respective Fe_2O_3-loaded carbons and 10 wt.% polytetrafluoroethylene (PTFE; Daikin Co.) and rolling. The Fe_2O_3-loaded carbon electrode was made into a pellet of 1 cm diameter. Cyclic voltammetry studies were carried out with a three-electrode glass cell assembly that had the Fe_2O_3-loaded carbon electrode as the working electrode, silver oxide as the counter electrode, Hg/HgO (1 M NaOH) as the reference electrode and cellophane, together with filter paper, as the separator, which was sandwiched by the two electrodes. The electrolyte used was 8 mol dm^{-3} aqueous KOH. Cyclic voltammetry measurements were recorded at a sweep rate of 0.5 mV s^{-1} and in the range of −1.2 to −0.1 V. After the 15th redox cycle, the Fe_2O_3-loaded carbon electrodes were removed, washed with deionized water, dried and observed by SEM-EDS so as to compare with the results of the electrodes before cycling.

The galvanostatic cycling performance measurements for the Fe_2O_3-loaded carbon electrodes were carried out with a three-electrode glass cell assembly. The discharge cut-

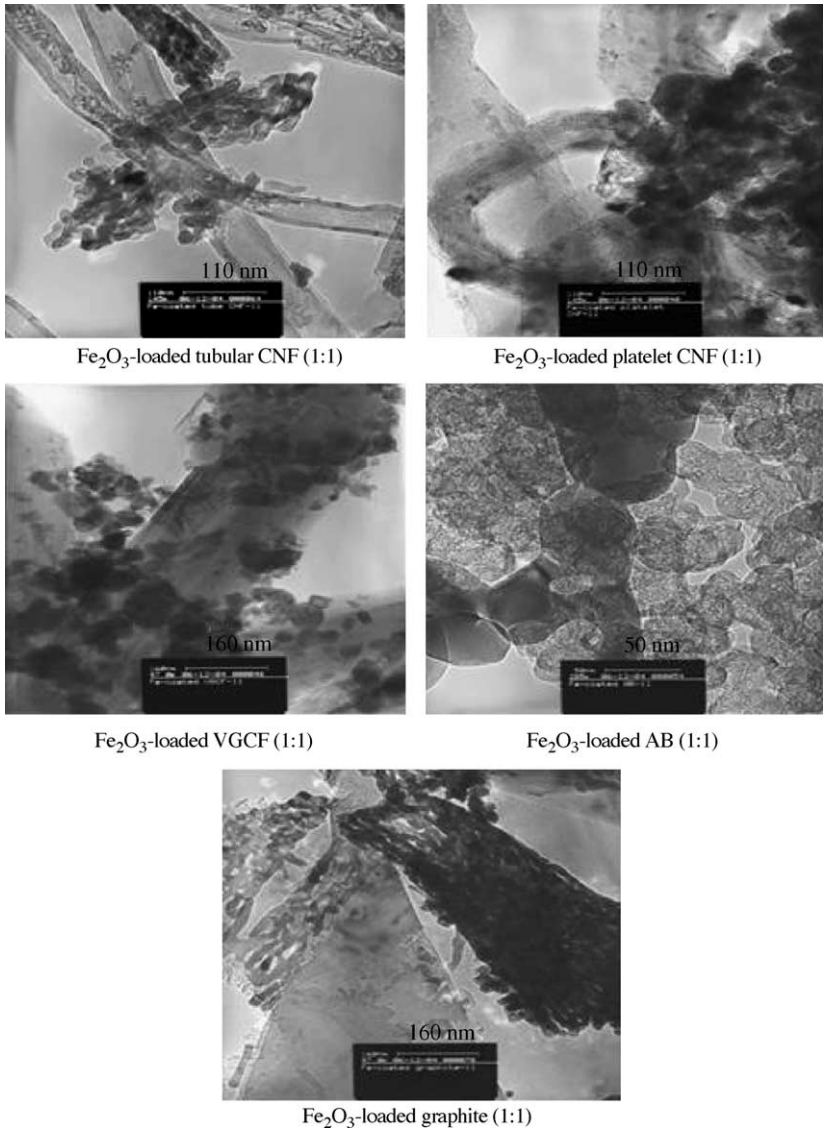

Fe_2O_3-loaded tubular CNF (1:1)

Fe_2O_3-loaded platelet CNF (1:1)

Fe_2O_3-loaded VGCF (1:1)

Fe_2O_3-loaded AB (1:1)

Fe_2O_3-loaded graphite (1:1)

Fig. 5. TEM images of the as-prepared Fe_2O_3-loaded carbon materials.

off potential was −0.1 V, and a constant potential charging step was applied at −1.15 V after the galvanostatic charging. The constant potential of −1.15 V was used because of the large amount hydrogen evolution observed at −1.2 V. The current densities for the charge and discharge process were employed in two different conditions. In the first condition, the charge and discharge current densities were both 1 mA cm^{-2}, and in the second condition the charge and discharge current densities were 0.5 and 0.2 mA cm^{-2}, respectively.

3. Results and discussion

The X-ray patterns of the Fe_2O_3-loaded AB and Fe_2O_3-loaded tubular CNF electrodes before and after the 15th cycle at different weight ratios of iron and carbon are presented in Fig. 1. It can be seen that for the Fe_2O_3-loaded carbon materials before cycling (Fig. 1a) at different weight ratios of iron and carbon, Fe_2O_3 is indeed present on the carbon surface. Therefore, the active material of the Fe_2O_3-loaded carbon materials is Fe_2O_3.

Figs. 2–4 depict the SEM images and distribution of Fe_2O_3 and carbon particles by EDS of as-prepared Fe_2O_3-loaded samples with tubular CNF, AB and graphite, respectively. The distribution of Fe_2O_3 and carbon on Fe_2O_3-loaded AB, Fe_2O_3-loaded tubular CNF and Fe_2O_3-loaded graphite materials revealed that Fe_2O_3 was well dispersed on the carbon surface. Such dispersion should increase the active material surface area and improve the redox reaction of iron.

In order to confirm the nature of the Fe_2O_3 present on the carbons, TEM measurements were carried out. TEM images of as-prepared Fe_2O_3-loaded carbons are shown in Fig. 5. The dark particles in this figure are Fe_2O_3. The TEM images demonstrated that fine Fe_2O_3 particles were dispersed on the carbon surface. Such a distribution of Fe_2O_3 is expected to improve the cycleability of the Fe_2O_3-loaded carbon electrodes during cycling. Comparison with Fe/C-mixed composite electrodes suggests that the Fe_2O_3-loaded carbons

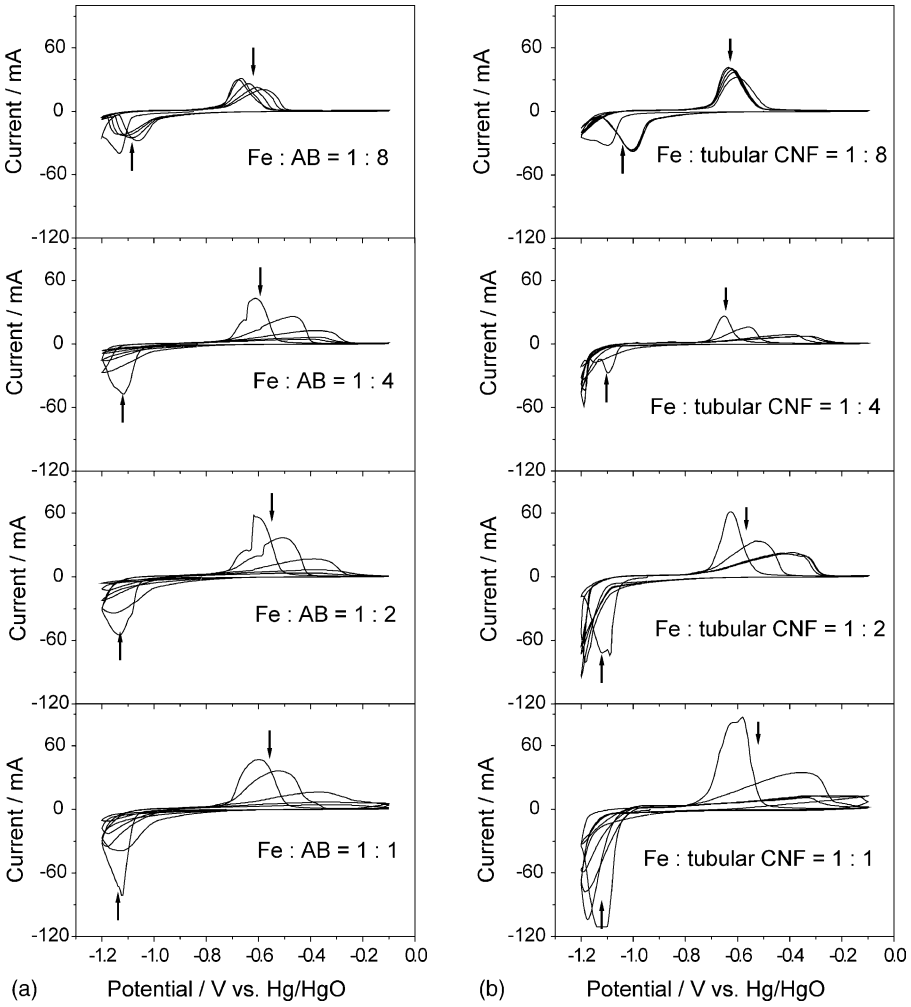

Fig. 6. Cyclic voltammetry of Fe_2O_3-loaded AB (a) and Fe_2O_3-loaded tubular CNF (b) electrodes at various weight ratios of iron-to-carbon (arrows present the tendency of the current during the cycling).

have larger active material surface areas than those of the Fe/C-mixed composite electrodes. Further, the active materials of the Fe/C-mixed electrodes consist of relatively large iron particles, viz., a few 10ths of a micrometer in contact with carbon. The method for preparing Fe/C-mixed composite electrodes has been described in our previous publication [23]. Thus, the Fe_2O_3-loaded electrodes are expected to provide larger capacity than those of the Fe/C-mixed composite electrodes.

The voltammograms of the Fe_2O_3-loaded carbon electrodes having weight ratios of iron-to-carbon of 1:1, 1:2, 1:4 and 1:8 during the initial five cycles are shown in Figs. 6–8 . Several peaks were observed, including the oxidation of Fe(II)/Fe(III) at around −0.6 V and the corresponding reduction peak at around −1.1 V. With further cycling, the anodic peak moved to a more positive potential, while the cathodic peak shifted toward a more negative potential, and the current under these peaks decreased. This suggests that the reaction was becoming irreversible, resulting in increased overpotential. The redox couple of Fe/Fe(II) was not observable. This could be ascribed to the insulating nature of the $Fe(OH)_2$ active material, which would inhibit the Fe/Fe(II) redox couple, causing a large overpotential. $Fe(OH)_2$ will be reduced to Fe at a lower potential than the cutoff potential of −1.2 V. The other possible reason is hydrogen evolution, occurring at around −1.1 V. In the first cycle, Fe_2O_3 was reduced to $Fe(OH)_2$ and then $Fe(OH)_2$ was oxidized to $Fe(OH)_3$ or FeOOH; with further cycling, this Fe(II)/Fe(III) redox couple became predominant, while the Fe/Fe(II) redox couple was insignificant. In order to check the presence of the Fe/Fe(II) redox couple, CV measurements were carried out on Fe_2O_3-loaded carbon electrodes with a reversal potential of −1.3 V (Fig. 9a); after the 15th cycle, the cathodic scan from −0.1 to −1.3 V was stopped at zero current in the potential range −1.1 to −0.9 V, and X-ray measurements were made. The XRD patterns of the Fe_2O_3-loaded AB and Fe_2O_3-loaded tubular CNF are shown in Fig. 1b. Fig. 9a indicates that the Fe/Fe(II) oxidation peak occurred during the cycling around −0.9 V with much smaller current compared with that of

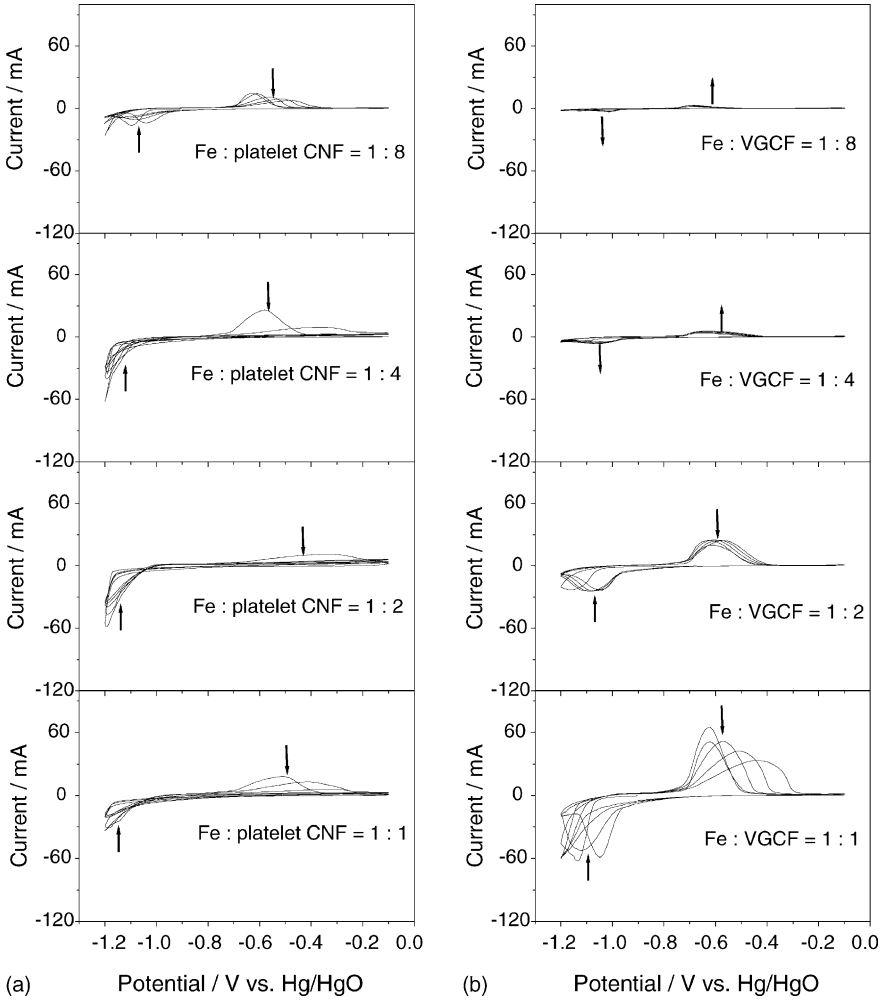

Fig. 7. Cyclic voltammetry of Fe_2O_3-loaded platelet CNF (a) and Fe_2O_3-loaded VGCF (b) electrodes at various weight ratios of iron and carbon (arrows present the tendency of the current during the cycling).

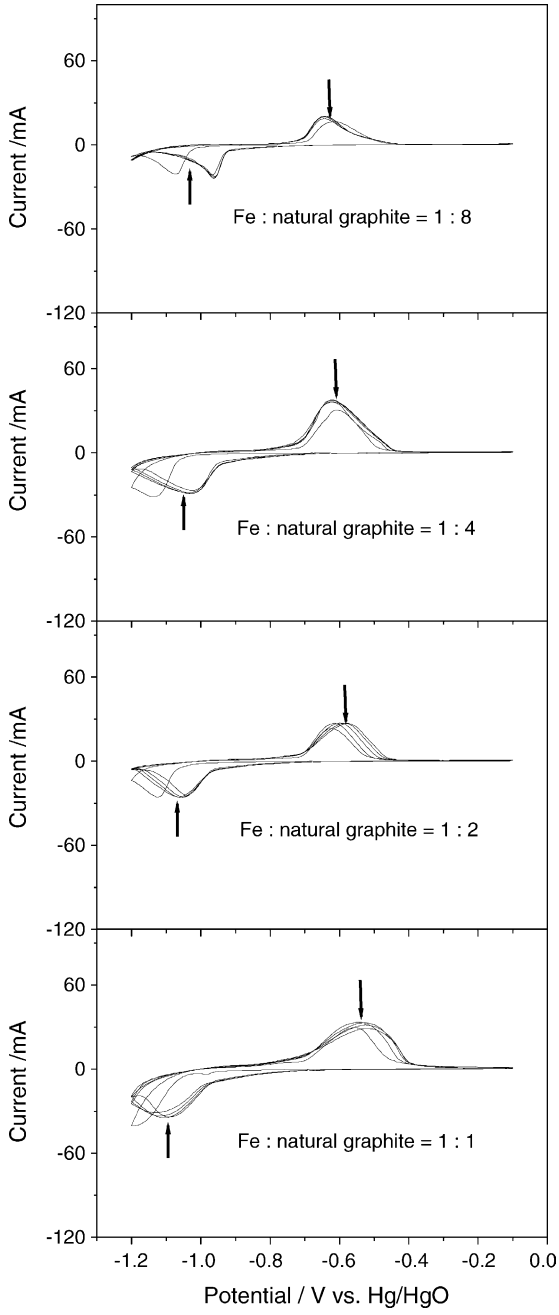

Fig. 8. Cyclic voltammetry of Fe_2O_3-loaded natural graphite electrode at various weight ratios of iron-to-carbon (arrows present the tendency of the current during the cycling).

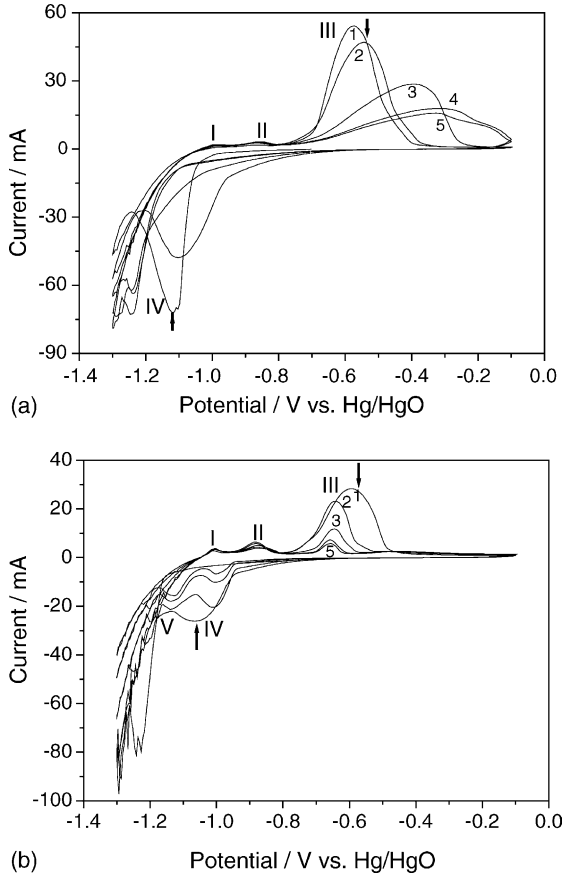

Fig. 9. Cyclic voltammetry of Fe_2O_3-loaded AB (Fe:AB:PTFE = 45:45:10 wt.%) (a) and Fe_2O_3-nano/AB-mixed (Fe_2O_3:AB:PTFE = 45:45:10 wt.%) (b) electrodes (arrows present the tendency of the current during the cycling).

Fe(II)/Fe(III) oxidation peak. However, the reduction peak of iron deposition was not separated from the hydrogen evolution peak. From Fig. 1b, it can be seen that Fe peaks are present on the carbon surface, thereby confirming that the Fe/Fe(II) redox process occurred during the cycling. However, this couple was not observed on further cycling, and this may be due to the insulating nature of $Fe(OH)_2$. To make clear the reason that the Fe/Fe(II) redox couple was not visible upon further cycling, another CV measurement was carried out on a Fe_2O_3-nano/C-mixed electrode (Fe_2O_3:C:PTFE = 45:45:10 wt.%) using Fe_2O_3 nanopowder (Aldrich), with an average diameter of ca. 2–3 nm. The result is shown in Fig. 9b. It is clear that both Fe/Fe(II) and Fe(II)/Fe(III) redox couples were observed. However, the redox current for the Fe/Fe(II) couple was much smaller than that of the Fe(II)/Fe(III) couple. Furthermore, the reduction peak of iron deposition occurred at a low potential (around −1.15 V) together with hydrogen evolution. Similar with the Fe_2O_3-loaded carbon electrode, the redox current decreased with increasing cycle number. These results revealed that the Fe_2O_3-loaded carbon electrodes had larger internal resistances than that of the Fe_2O_3-nano/C-mixed electrode, leading to the disappearance of the Fe/Fe(II) redox couple.

As is evident from Figs. 6–8, the type of carbon used, as well as the ratio of iron-to-carbon, affect the redox behavior of iron. For all carbons, except natural graphite, when a large amount of Fe_2O_3 was loaded, for example, when the ratios between iron and carbon were 1:1, 1:2 and 1:4 (Fig. 10), the redox current decreased rapidly with repeated cycling, while the 1:8 ratio showed better retention of redox current. Further,

when the material used was natural graphite (Fig. 10), the current decreased gradually for all the different ratios between iron and carbon. The decrease in redox current may be explained based on the $Fe(OH)_2$ layer formed during the cycles, resulting in passivation. When a larger amount of Fe_2O_3 was loaded on the carbon, the $Fe(OH)_2$ layer should be thicker, thereby resulting in a rapid decrease of the redox current on cycling. Additionally, the morphology of the carbon affects the redox behavior of the Fe_2O_3-loaded carbon electrode. For example, tubular CNF exhibits the largest current at a 1:1 ratio, compared with other carbons, although this current decreased rapidly on further cycling, while platelet CNF provided the smallest current at different ratios. Similar to tubular CNF, AB showed larger redox current at the first cycle than that of VGCF or platelet CNF or graphite at all ratios, but this current decreased quickly. Although VGCF showed large currents at high Fe_2O_3 loadings, viz., ratios of 1:1 and 1:2, the redox current obtained was very small at low Fe_2O_3 loading and increased with increasing cycle number. This behavior is acceptable, looking from the viewpoint of nano-carbons, especially tubular CNF and AB, which have larger actual surface areas than other carbons (Table 1). Consequently, Fe_2O_3 was more dispersed on tubular CNF and AB than other carbons, and the thickness of the $Fe(OH)_2$ layer on tubular CNF and AB was also thinner than on other carbons. Such dispersion results in a larger active surface area for Fe_2O_3-loaded tubular CNF and Fe_2O_3-loaded AB electrodes than other Fe_2O_3-loaded carbon electrodes, thereby supporting the redox reaction of iron. However, the redox current decreased, even in the case of Fe_2O_3-loaded tubular CNF and Fe_2O_3-loaded AB on repeated cycling. This may be due to a dissolution–deposition mechanism, which would result in an intermediate species, i.e., $HFeO_2^-$ [7,16], to be re-distributed on the carbon surface. In order to confirm the distribution of iron on the carbon surface, SEM and EDS studies were carried out with Fe_2O_3-loaded AB and Fe_2O_3-loaded graphite after the 15th cycle and are presented in Fig. 11. Comparing the SEM and EDS before cycling (Figs. 3–4), it is clear that after cycling, the iron was aggregated into large particles on the carbon surface, and this could be the reason for the decrease of redox current on further cycling.

Comparison of cyclic voltammetric (CV) results of Fe_2O_3-loaded carbon electrodes at corresponding ratios, for all of the carbons, indicates that the iron-to-carbon ratio of 1:8 appears to give excellent, long cycle life for Fe_2O_3-loaded carbon materials. Fig. 12 presents the CV profiles of Fe_2O_3-loaded carbon electrodes at five initial cycles having 1:8 ratios for iron–carbon compared with the corresponding Fe/C-mixed composite electrodes (Fe:C:PTFE = 10:80:10 wt.%). It is interesting to note that in the case of Fe/C-mixed electrodes, the current increased on cycling as compared

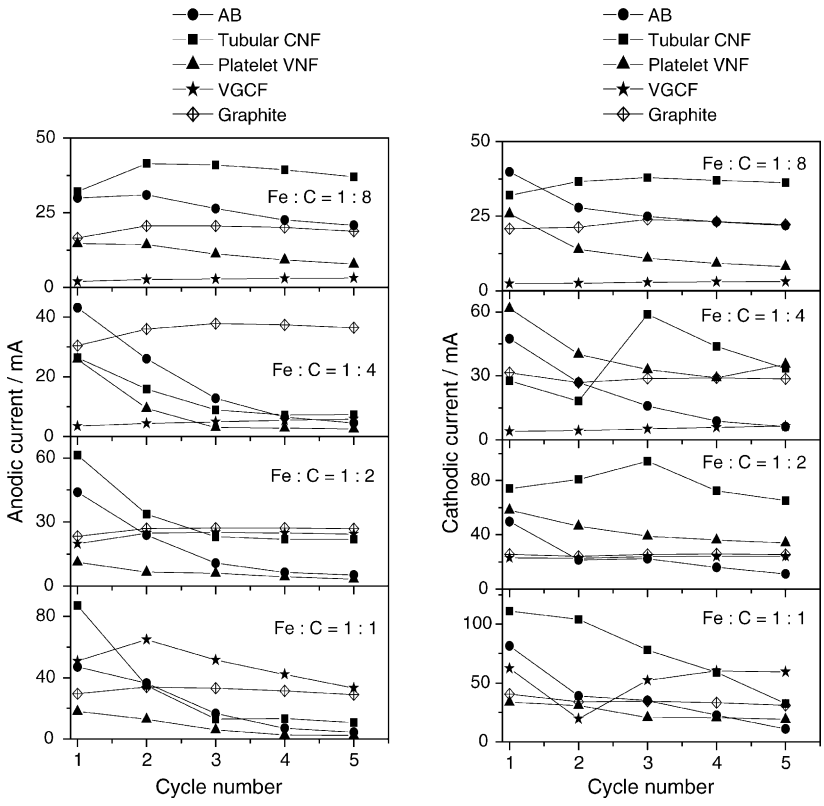

Fig. 10. Variation of redox current of Fe_2O_3-loaded carbon electrodes with the cycle number.

to Fe_2O_3-loaded carbon electrodes. The origin of the increase in current has already been explained in our previous work [23]. However, the Fe_2O_3-loaded carbon electrodes show much larger redox current than those for the Fe/C-mixed electrodes in the initial cycles. Comparison of all carbons employed for the preparation of Fe_2O_3-loaded electrodes indicates that the tubular CNF, AB and graphite exhibited larger currents than VGCF and platelet CNF.

The cycle performance of Fe_2O_3-loaded carbons is presented in Fig. 13. When a higher current density was applied for the charge and discharge process (Fig. 13a), the capacities of all of the Fe_2O_3-loaded carbon electrodes were smaller than those of the Fe_2O_3-loaded carbon electrodes using lower current density (Fig. 13b). The decrease in capacity of Fe_2O_3-loaded platelet CNF was present clearly when using high current density for the charge/discharge process. When the lower current density was used for the charge/discharge process (Fig. 13b), the capacities were improved. The initial cycles for the Fe_2O_3-loaded carbon electrodes, excluding that of Fe_2O_3-loaded VGCF, showed large discharge capacities, but these subsequently decreased. However, Fe_2O_3-loaded VGCF showed stable capacities for the initial cycles, and then these stable capacities decreased slightly with increasing cycle number. Comparison with other Fe_2O_3-loaded carbons indicates that Fe_2O_3-loaded VGCF delivered the smallest discharge capacity in the initial cycles, but after long cycling, the Fe_2O_3-loaded platelet CNF and Fe_2O_3-loaded AB had smaller capacities than other electrodes. For both current densities employed, graphite showed the best discharge capacity among the carbon materials used. Tubular CNF delivered a slightly smaller capacity than graphite after long cycling but larger than AB. This order was different with the CV measurements, which revealed that tubular CNF showed the largest redox current. This may be due to the experimental conditions for this measurement. However, the tendency of decrease in discharge capacity for the Fe_2O_3-loaded carbon electrodes agrees with the CV results. The main reason is the formation of $Fe(OH)_2$ during the charge/discharge, with the latter resulting in the passivation of the electrode. In order to obtain the best performance for Fe_2O_3-loaded carbon electrodes, the preparation of the electrodes and the charge–discharge conditions are to be further investigated in a future study.

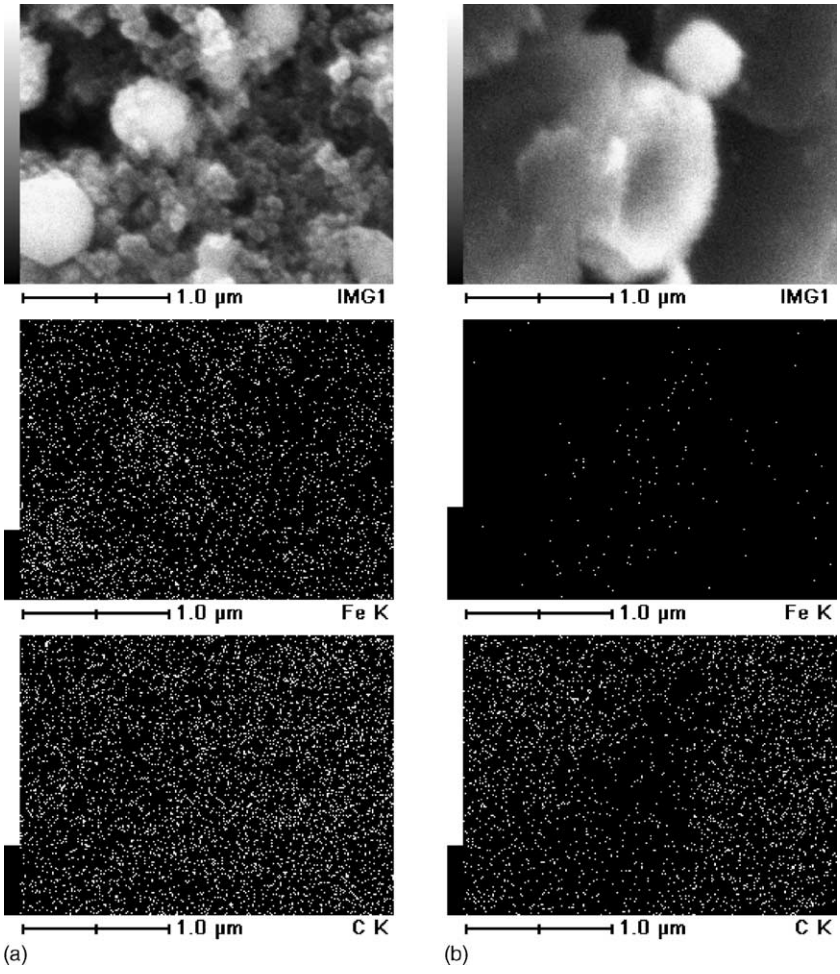

Fig. 11. SEM images and distribution of iron and carbon of Fe_2O_3-loaded AB (a) and Fe_2O_3-loaded natural graphite (b) electrodes after the 15th redox cycle.

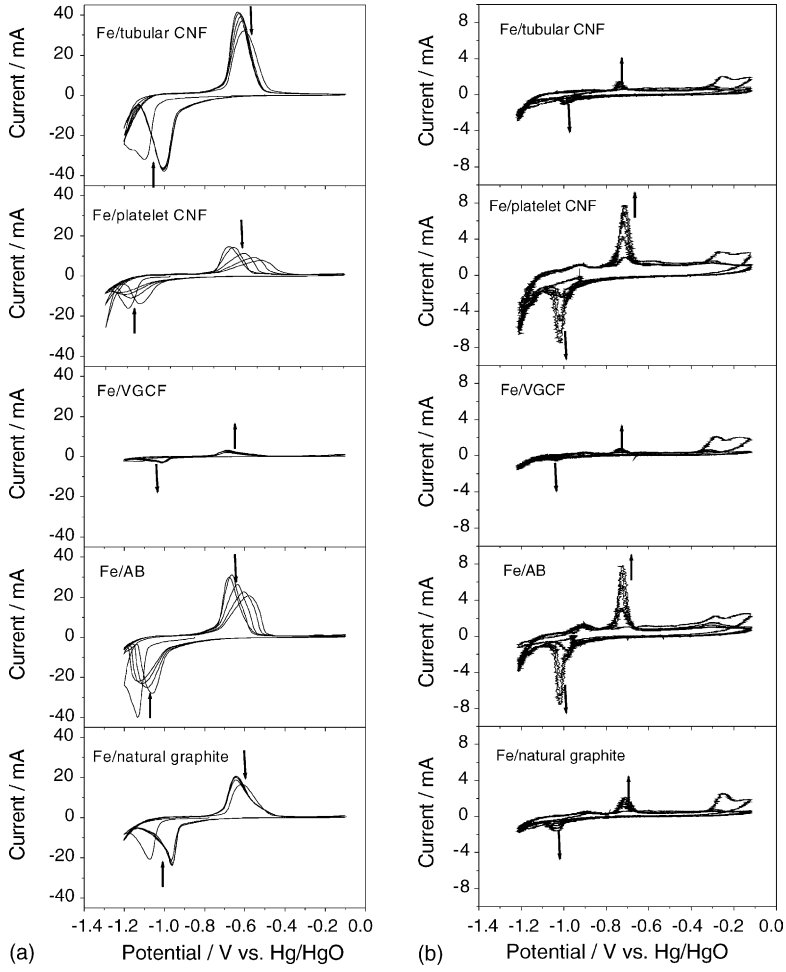

Fig. 12. Cyclic voltammetry of Fe_2O_3-loaded carbon (Fe:C:PTFE = 10:80:10 wt.%) (a) and Fe/C-mixed composite (Fe:C:PTFE = 10:80:10 wt.%) (b) electrodes for five initial cycles (arrows present the tendency of the current during the cycling).

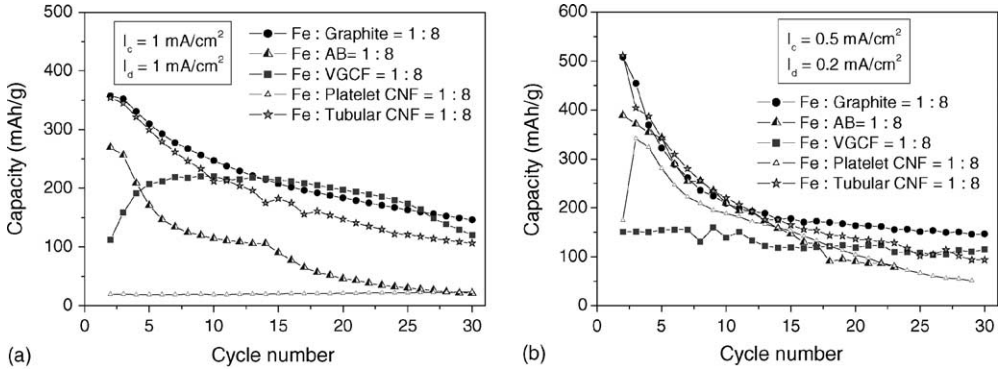

Fig. 13. Cycle performance of Fe_2O_3-loaded various carbon electrodes in 8 M KOH solution: (a) high charge and discharge current density; (b) low charge and discharge current density.

4. Conclusions

The type of carbon used and the ratio between iron and carbon play important roles in determining the electrochemical properties of Fe_2O_3-loaded carbon electrodes. The best performance for Fe_2O_3-loaded carbon electrodes can been observed for an iron–carbon ratio of 1:8. Higher redox currents are obtained for Fe_2O_3-loaded nano-carbon electrodes employing acetylene black and tubular CNF. The redox current decreased initially and stabilized after several charge/discharge cycles. VGCF although showed the smallest current among nano-carbons at an iron–carbon ratio of 1:8, but the current increased with increasing cycle, thereby resulting in stable capacity during the charge/discharge cycles.

The Fe_2O_3-loaded graphite electrode showed the smaller redox current compared with those of the Fe_2O_3-loaded AB or Fe_2O_3-loaded tubular CNF electrodes, but the redox current decreased marginally with increasing numbers of cycles, thereby resulting in large capacity.

Comparison of Fe/C-mixed and Fe_2O_3-loaded carbon electrodes indicates that higher capacities are obtained in the latter case due to the highly uniform distribution of iron on the carbon surface.

Acknowledgement

This work was supported by the CREST program of JST (Japan Science & Technology Agency).

References

[1] L. Ojefors, L. Carlsson, J. Power Sources 2 (1977/1978) 287–296.
[2] K.F. Blurtin, A.F. Sammells, J. Power Sources 4 (1979) 263–279.
[3] A.M. Kannan, A.K. Shukla, J. Power Sources 35 (1991) 113–121.
[4] A.J. Salkind, C.J. Venuto, J. Electrochem. Soc. 111 (1964) 493–495.
[5] H.G. Silver, E. Lekas, J. Electrochem. Soc. 117 (1970) 5–8.
[6] L. Ojefors, J. Electrochem. Soc. 123 (1976) 824–828.
[7] L. Ojefors, J. Electrochem. Soc. 123 (1976) 1691–1696.
[8] R.S. Schrebler-Guzman, J.R. Viche, A.J. Arvia, Electrochim. Acta 24 (1979) 395–403.
[9] V.S. Muralidharan, M. Veerashanmugamani, J. Appl. Electrochem. 15 (1985) 675–683.
[10] G.P. Kalaignan, V.S. Muralidharan, K.I. Vasu, J. Appl. Electrochem. 17 (1987) 1083–1092.
[11] N. Jayalakshimi, V.S. Muralidharan, J. Power Sources 32 (1990) 277–286.
[12] M.D. Koninck, T. Brousse, D. Belanger, Electrochim. Acta 48 (2003) 1425–1433.
[13] J. Cerny, J. Power Sources 25 (1989) 111–122.
[14] D.W. Shoesmith, P. Taylor, M.G. Bailey, B. Ikeda, Electrochim. Acta 23 (1978) 903–916.
[15] T.S. Balasubramanian, A.K. Shukla, J. Power Sources 41 (1993) 99–105.
[16] P. Periasamy, B.R. Babu, S.V. Iyer, J. Power Sources 58 (1996) 35–40.
[17] P. Periasamy, B.R. Babu, S.V. Iyer, J. Power Sources 63 (1996) 79–85.
[18] C.A. Caldas, M.C. Lopes, I.A. Carlos, J. Power Sources 74 (1998) 108–112.
[19] P. Schmuki, M. Buchler, S. Virtanen, H.S. Isaacs, M.P. Ryan, H. Bohni, J. Electrochem. Soc. 146 (1999) 2097–2102.
[20] I. Diez-Perez, P. Gorostiza, F. Sanz, J. Electrochem. Soc. 50 (2003) B348–B354.
[21] M.D. Koninck, D. Belanger, Electrochim. Acta 48 (2003) 1435–1442.
[22] Z. Ding, C. Yang, Q. Wu, Electrochim. Acta 49 (2004) 3155–3159.
[23] B.T. Hang, M. Egashira, I. Watanabe, S. Okada, J. Yamaki, S. Yoon, I. Mochida, J. Power Sources, 2005, in press.